ELSEVIER

Journal of Chromatography A, 788 (1997) 173–183

JOURNAL OF CHROMATOGRAPHY A

High resolution multichannel fluorescence detection for capillary electrophoresis Application to multicomponent analysis

Kurt E. Oldenburg, Xiaoyan Xi, Jonathan V. Sweedler*

Department of Chemistry, Beckman Institute, University of Illinois at Urbana-Champaign, Urbana, IL 61801, USA

Received 17 March 1997; received in revised form 11 June 1997; accepted 20 June 1997

Abstract

A wavelength-resolved fluorescence detector for laser-induced fluorescence detection in capillary electrophoresis (CE) is described that uses a charge injection device (CID) array detector. Post-column fluorescence detection occurs using a sheath flow cell. The limit of detection for fluorescein is $4.8 \cdot 10^{-11}$ *M* (29 000 molecules), the spectral resolution is 0.56 nm/pixel, and the spectrograph/CID monitors a 250 nm spectrum throughout the 250–875 nm range. Custom array readout, data manipulation and data processing methods are described to convert wavelength/spatial CID images into electropherograms. The application of the system to characterizing bilirubins in human serum is described, demonstrating the ability to match electrophoretic peaks to standards using spectral information. © 1997 Elsevier Science B.V.

Keywords: Charge injection device array detection; Detection, electrophoresis; Fluorescein; Bilirubins

1. Introduction

In recent years, capillary electrophoresis (CE) has become a highly efficient separation technique well suited for the analysis of mass and volume limited samples [1–4]. CE is ideally suited for volume limited assays such as single cell analysis [5–8]. One of the challenges for separations of these complex samples is the detection and identification of the peaks in the electropherogram. Thus, the development of sensitive and information rich detectors is important.

The lowest limits of detection (LODs) reported for CE are based on laser-induced fluorescence (LIF) [9–11]. LIF LODs are improved through the use of sheath flow assemblies [10,12–15]. The separated analytes are detected post-capillary in a stream of buffer flowing through a high purity quartz cuvette. In this configuration, capillary luminescence background is eliminated and the signal of interest is removed spatially from light scattered at the air–quartz and quartz–water interfaces. Chen et al. [10] have used sheath flow cells extensively for CE-LIF detection, and have reported a LOD value for sulforhodamine-101 of 6 molecules.

For many experiments, traditional electropherograms of signal as a function of elution time do not provide adequate information. If the sample mixture is complex, additional data about each analyte is desirable to aid in peak identification, analyte quantitation and assessment of peak purity. The most common detection scheme used to increase the

*Corresponding author.

0021-9673/97/$17.00
PII S0021-9673(97)00713-9

information content of CE is diode-array absorbance detection (DAD) [16–18]. The spectroscopic data DAD provides about the separation helps with the issues mentioned above, but low sensitivity can severely limit its applicability. Due primarily to the small path length through the capillary, concentration LOD values for commercial CE-DAD instruments are typically micromolar [2,3].

Through the use of imaging spectrographs and array detectors it is possible to combine spectral information with the sensitivity of LIF detection. Wavelength-resolved fluorescence detection using a photodiode array was first performed by Swaile and Sepaniak [19]. The use of charge coupled device (CCD) detectors helped improve performance of wavelength-resolved fluorescence detection through decreased detector noise, increased duty cycle and improved quantum efficiency [11,20–22]. A number of these systems, however, have had rather poor spectral resolution (effectively>4 nm/pixel after binning [19,20]) making the observation of small changes in fluorescence emission spectral profile difficult. The development and application of wavelength-resolved fluorescence detection for CE have been recently reviewed in greater detail elsewhere [23].

We have developed a high resolution (0.56 nm/pixel) wavelength-resolved fluorescence detector with a sheath flow assembly and commercial CE injection system, resulting in a flexible and sensitive system that provides enhanced information content about the separation. Fluorescein and fluorescein isothiocyanate derivatized amino acids are used to characterize the separation and detection performance of the system. The data processing techniques for wavelength-resolved fluorescence data are described, from focusing and data array selection, through two-dimensional data acquisition and post-run data analysis. The analysis of bilirubin in human serum is used to demonstrate how spectral information can help in peak purity determination and analyte identification from a complex sample.

2. Experimental

2.1. Electrophoresis system

The CE system uses a commercial CE autoinjector (Crystal 300, Thermo CE, Franklin, MA, USA) to inject sample and to apply the separation voltage. The Crystal performs highly reproducible injections (<1% R.S.D. of peak heights between repeated injections). Positive applied pressure at the inlet vial is used for all injections. Using the Poiseuille equation [2,3], the injected volume is calculated to be 1.1 nl. During injection and the first 30 s of the separation, the sheath flow buffer is stopped to prevent injection bias due to pressure effects [24]. To accomplish this, the CE instrument controls a solenoid valve (Cole Parmer, Niles, IL, USA) through an external event relay switch. The 65 cm× 50 μm I.D.×360 μm O.D. fused-silica capillary (Polymicro Technologies, Phoenix, AZ, USA) passes out of the CE injector and into a grounded aluminum assembly to which the quartz flow cell (NSG Precision Cells, Farmingdale, NY, USA) is mounted (see Fig. 1). The cell has 2 mm thick walls with 3×3 mm inner dimensions. Sheath flow buffer of the same composition as the running buffer flows gravimetrically through the cell at a rate that matches the average linear velocity of the fastest analyte eluting during a given experiment. This is done to minimize any deleterious effects of the sheath flow on the separation efficiency. All separations are performed with +25 kV applied potential at the inlet end of the capillary, except as noted. The mechanics of interfacing a sheath flow cell with CE has been described in greater detail elsewhere [13,14].

2.2. Detection system

As shown in Fig. 2, an argon ion laser (Innova FReD 300, Coherent, Palo Alto, CA, USA) is used for visible excitation at 488 nm. The beam from the laser is focused into the quartz flow cell with a 30 mm focal length fused-silica plano-convex lens (Spindler and Hoyer, Milford, MA, USA). To provide the optimum signal, the beam is positioned approximately 100 μm beneath the capillary outlet. The lens position is adjusted to insure that the beam is centered and approximately the same diameter as the capillary effluent.

The fluorescence signal is collected at a 90° angle relative to the excitation beam by a 15× all-reflective microscope objective (Opticon, Billerica, MA, USA). This optic collects light at $f/1.2$ with a 20% center obscuration and has an infinite conjugate ratio.

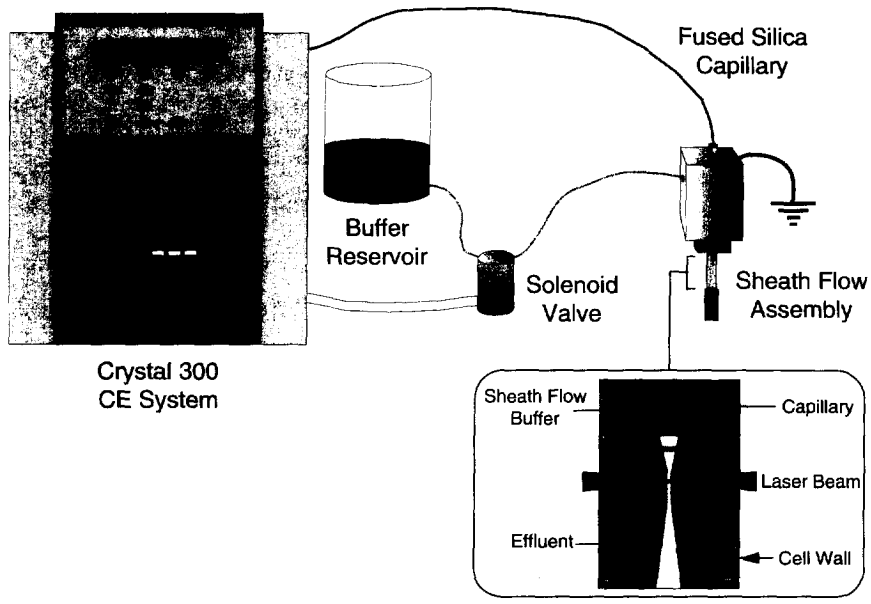

Fig. 1. Diagram of the CE system showing the Thermo CE instrument and the sheath flow assembly, as well as the sheath flow buffer reservoir and solenoid valve used to turn the sheath flow on or off.

The collected light is focused onto the entrance slit of an $f/8$, 0.5 m focal length imaging spectrograph (IS500, Chromex, Albuquerque, NM, USA) using an 80 mm focal length fused-silica plano-convex lens (Spindler and Hoyer) to insure $f/$ matching. This combination provides an overall magnification of approximately 8×.

The computer-controlled spectrograph has a number of features that are useful for this application. The motorized entrance slit can be adjusted from 0 to

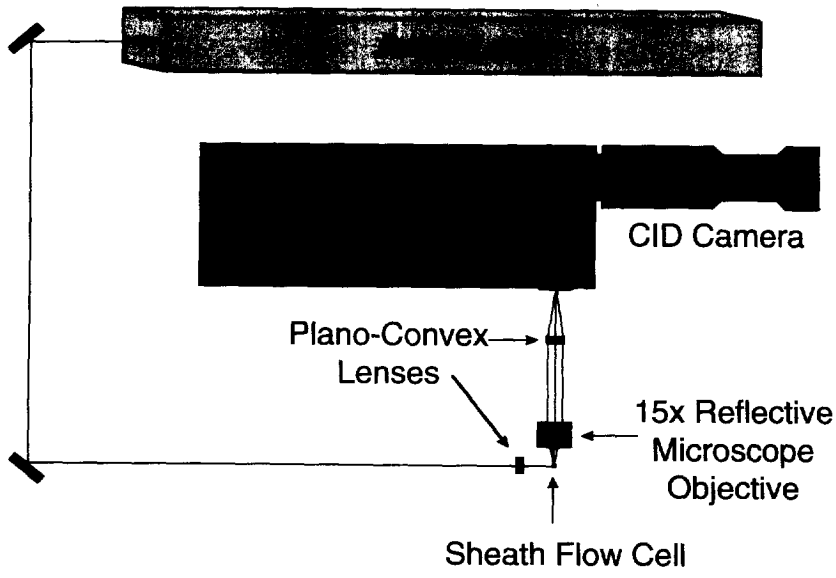

Fig. 2. Diagram of the fluorescence detection system showing the arrangement of the optics, spectrograph and laser.

2000 μm with a precision of ±2 μm. For these experiments the slit is set to 400 μm to match the magnified image of the sheath flow stream. The spectrograph has a motorized turret on which two gratings are mounted. This allows for the dispersed light to be positioned on the detector so the maximum possible emission wavelength range is observed and provides the ability to change gratings through software control. In addition to the 100 grooves/mm ruled grating blazed at 450 nm used in these experiment, a 150 grooves/mm holographic grating blazed at 250 nm is available for UV fluorescence experiments.

A 512×512 pixel charge injection device (CID) detector (SICAM SCM5000E, CIDTEC, Liverpool, NY, USA) is attached to the spectrograph using a custom mount made by the spectrograph manufacturer. Although they are used less commonly for scientific applications, CIDs have a number of advantageous characteristics; these include pseudo-random pixel addressing, non-destructive readouts (NDROs) to reduce read noise, high quantum efficiency, large linear response range and non-blooming pixels [25–28]. The camera is cooled with liquid nitrogen for all experiments to reduce the dark current. Camera control and data acquisition software is written in LabVIEW (National Instruments, Austin, TX, USA) on a PC compatible, 60 MHz Pentium computer (Gateway 2000, North Sioux City, SD, USA) using low-level function drivers provided by the CID manufacturer. Based on the reciprocal linear dispersion of the grating used in the spectrograph and pixel size of the CID camera, the resolution is 0.56 nm/pixel.

2.3. Reagents

To minimize the presence of chemical impurities, ultra-pure Milli-Q water (Millipore, Bedford, MA, USA) is used to prepare all solutions. Buffer solutions are filtered using 0.2 μm syringe filters (Gelman Sciences, Ann Arbor, MI, USA) to remove particulates. All separations, except as noted, are performed using 50 m*M*, pH 9.1 borate buffer. This buffer is prepared by dissolving 3.09 g of boric acid and 7.91 g of sodium tetraborate decahydrate (EM Science, Gibbstown, NJ) in Milli-Q water and diluting the solution to a final volume of 1 l. The buffer is degassed by ultrasonication for 30 min prior to use to minimize the formation of bubbles in the separation capillary and sheath flow cell.

All fluorescein solutions used are made by serial dilutions from a stock solution of 0.1 m*M* fluorescein (Sigma, St Louis, MO, USA) in borate buffer. For derivatization of amino acids, a 0.5 m*M* solution of fluorescein isothiocyanate (FITC) in spectroanalytical grade methanol (Aldrich, Milwaukee, WI, USA) is prepared. Solutions of 1 m*M* arginine (Arg), proline (Pro), asparagine (Asn) and glycine (Gly) (cell culture grade, Sigma) solutions are made in Milli-Q water. The amino acids are derivatized by mixing 1 ml of the FITC solution with 0.5 ml of the individual solutions and 2.5 ml of borate buffer. After vortexing, the mixtures are allowed to react for 15 h in the dark at room temperature. A mixture containing 1:4000 dilutions of the FITC derivatized Arg, Pro and Gly and 1:2000 dilution of derivatized Asn in borate buffer is prepared.

For the spectral differentiation of bilirubin in human serum, total bilirubin in human albumin standard, and frozen normal human serum (both from Sigma) are used. The bilirubin standard has a total bilirubin concentration of 9 mg/dl, but assayed values for individual isomers are not available. Both the standard mix and the human serum are analyzed without dilution using +30 kV separation potential. The running buffer consists of 40 m*M* sodium dodecyl sulfate (SDS) (Sigma) and 5% by volume acetonitrile (spectroanalytical grade, Aldrich) in 50 m*M*, pH 9.1 borate buffer.

3. Data processing and analysis

3.1. System optimization and data acquisition

Although the addition of wavelength-resolution to LIF provides increased information content, acquiring and processing the separation data presents a number of challenges. Some of which are: optimization of the fluorescence signal, acquisition of large spectral arrays while maintaining a high duty cycle, determination of separation and detection performance characteristics and analysis of spectral data.

Prior to performing separations, the optics of the system are focused by maximizing the image intensi-

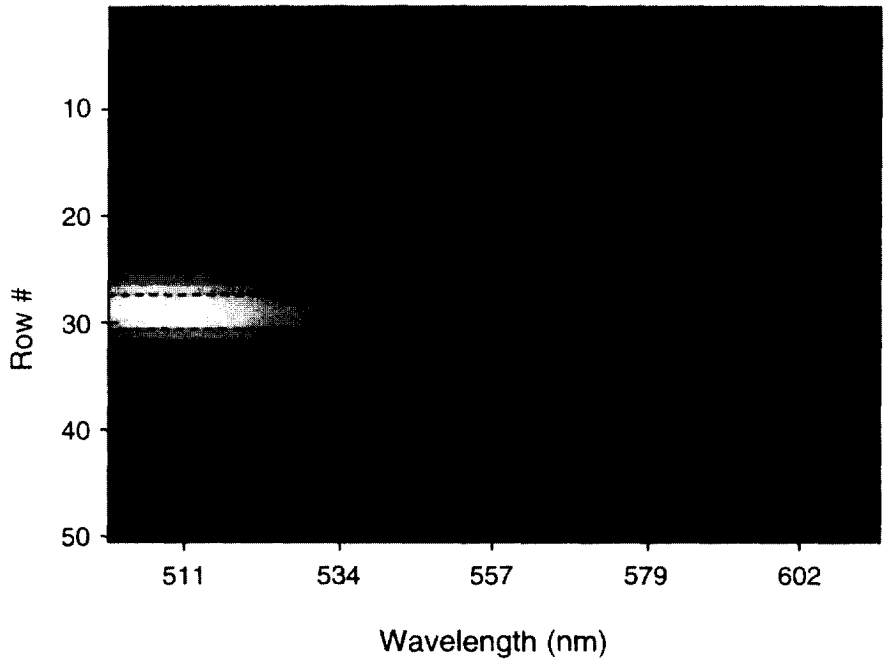

Fig. 3. Direct image from the CID/spectrograph, where one axis of the CID contains a one-dimensional image of the sheath flow cell and the other is spectral information. The image is obtained when 10^{-7} *M* fluorescein is flowing from the CE capillary, and the two lines mark the spatial regions where the CID is read during an electrophoresis separation.

ty for a constant flow of fluorescein solution, as shown in Fig. 3. As indicated on this image, a sub-array containing a portion of the fluorescence signal is selected for the separation run. This sub-array is empirically selected so that the optimum signal-to-noise ratio is provided during the acquisition of separation data. By binning several rows of detector elements, the intensity of a given spectrum can be increased. However, with addition of each row the baseline noise is also increased, so the use of low intensity spectra can be detrimental to the signal-to-noise ratio of the resulting spectral sum. The spectral range observed is dependent on the sample being analyzed. The lowest number of wavelength elements that will provide sufficient spectral information for the given sample is selected to maximize the duty cycle of the detector and minimize the size of the final data file. Typically, the sub-array used contains 3 to 5 rows by 50 to 500 columns, corresponding to a 12 to 18 μm area of the sheath flow cell and a 28 to 280 nm spectral range, respectively.

As mentioned above, the use of sheath flow assemblies eliminate many sources of background noise. In our instrument, the major source of noise is detector noise. To reduce the effective read noise of the CID, NDROs are performed during separations. The number of NDROs that provides the best compromise between noise reduction and decreased duty cycle for our application is 4, resulting in a 50% decrease in read noise since the noise decreases by the square root of the number of reads. The resulting duty cycle for this number of NDROs on a sub-array selected as described above is >75%.

Manipulation and storage of array data can use extensive memory and processing resources, which can impact the data acquisition timing precision. To avoid this, arrays of data from the CID are streamed to a temporary storage file on the hard drive of the controlling computer immediately after acquisition. When the run is complete, the temporary file is processed by averaging the NDROs of each pixel and then binning the rows of the individual reads. The completely processed data file is a two-dimensional array containing (acquisition rate)*(run time)

individual emission spectra (see Fig. 4A). The acquisition rate for all experiments reported here is 1 Hz. These files are then analyzed on an IBM RS/6000 workstation (IBM, White Plains, NY, USA) using custom routines written in IBM Visualization Data Explorer (IBM Research, Yorktown Heights, NY, USA) and MATLAB (MathWorks, Boston, MA, USA).

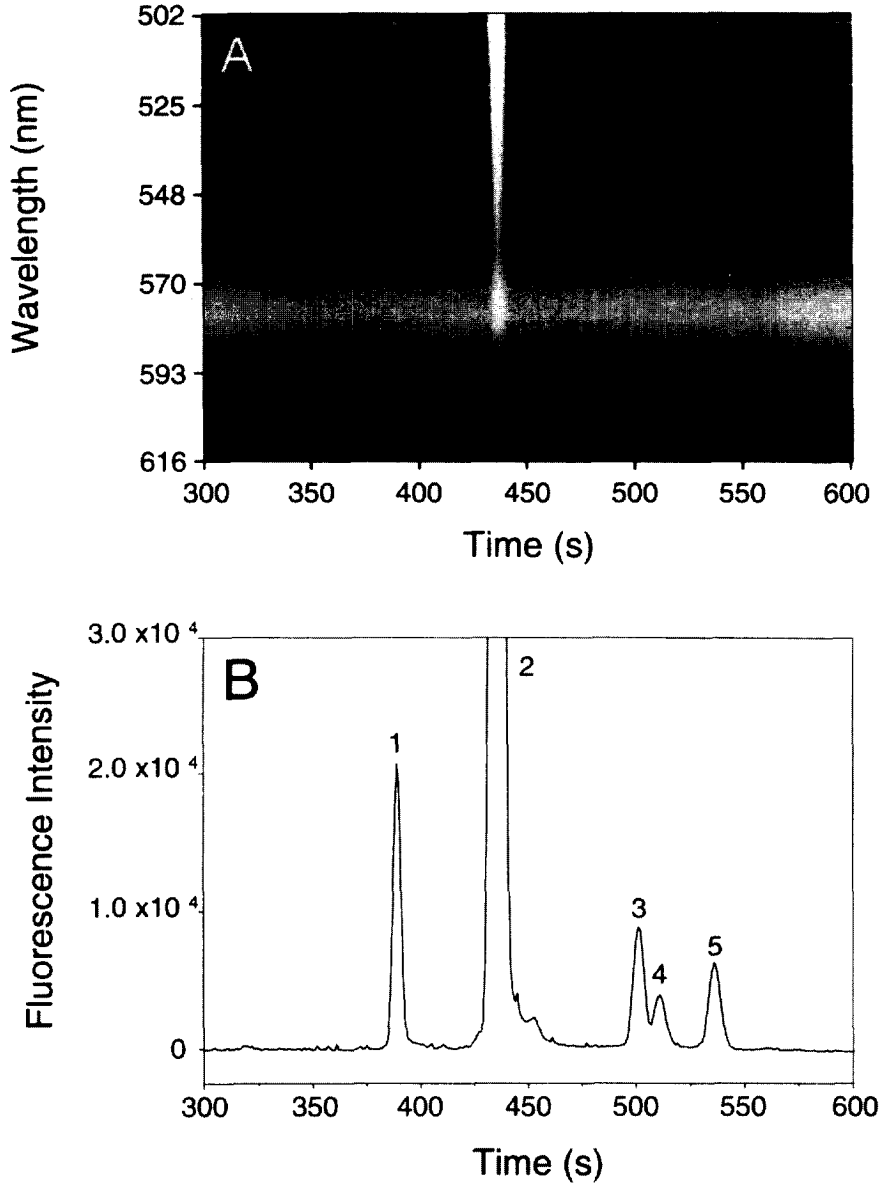

Fig. 4. (A) Two-dimensional electropherogram of a mix of FITC-labeled amino acids where the region marked in Fig. 3 is summed during each CID readout. The continuous band centered at 575 nm is the major Raman band of water, and the vertical bands are from the fluorescence components eluting at specific times. The two horizontal lines indicate the wavelength regions to be summed to reduce the data to a one-dimensional electropherogram. (B) Resulting one-dimensional electropherogram of the labeled amino acids: 1 = 15 n*M* Arg, 2 = FITC, 3 = 13 n*M* Pro, 4 = 10 n*M* Asn and 5 = 14 n*M* Gly.

3.2. Detection limit and separation efficiency calculations

LODs and separation efficiencies are determined using custom automated routines written in MATLAB. First, a one-dimensional electropherogram is created from the two-dimensional data set by summing a small range of wavelengths near the emission maximum of the analyte of interest (see Fig. 4B). The wavelengths used, covering about 15 nm centered at 514 nm for fluorescein, are selected to obtain the optimal signal-to-noise ratio for a given analyte. In this manner, the wavelength information is used in a similar manner as would an interference filter to eliminate unwanted signal. The advantage of this method is that the wavelengths can be adjusted dynamically depending on the particular components present (i.e., the spectral background present from various buffer additives may change the optimum wavelengths). The electropherogram is next processed, if necessary, to remove signal spikes caused by small air bubbles in the sheath flow as they pass through the detection region. These events are easily identifiable as single time interval occurrences of high signal intensity. Each data point is checked to determine if it is a spike by calculating the mean and standard deviation of six points that surround it. If the intensity exceeds the mean by more than a threshold number of standard deviations, typically seven, the value of that point is replaced by the mean value. Next, the baseline noise is calculated using a portion of the electropherogram containing at least 50 points just prior to the peak in question. A least-squares regression of this data provides the average baseline, and the root-mean-squared deviation of the data from this line is the noise (σ). Peaks are identified by finding data points that have intensities greater than 3σ when calculated from the least squares baseline and that are higher in intensity than the two adjacent points. This insures that the true maximum of the peak is found. The signal-to-noise ratio for the peak is determined by dividing the peak height calculated from the least squares baseline by σ, and the LOD is calculated by extrapolating from this value the concentration that would yield a peak with an intensity of 3σ.

Separation efficiencies are calculated by a Gaussian fitting routine. The peaks are modeled as Gaussian curves of intensity as a function of time. A section of the electropherogram containing the peak of interest is fit to the function using a simplex optimization function in MATLAB to calculate the equation parameters that minimize the squared difference between the fit and experimental data. Using the value of σ calculated in this manner, the theoretical plates of the peak can in turn be determined.

3.3. Background subtraction, data smoothing and spectral analysis

For spectral analysis and comparison, background subtraction must be performed to eliminate the Raman signal of water and the fixed background pattern of the CID. A 100 read section of the two-dimensional electropherogram that does not contain analyte peaks or signal spikes is averaged using MATLAB to provide a background spectrum. Using this single spectrum, an array containing the appropriate number of spectra is assembled and subtracted from the two-dimensional electropherogram. Signal spike removal can be performed on the two-dimensional data in a method similar to that used for one-dimensional electropherograms. The calculations described above are repeated along each wavelength row of the data array. If data smoothing is required to improve the signal-to-noise ratio of the data, the two-dimensional electropherogram is convolved with a filter matrix and normalized to yield a new array [29]. The spectrum of a given peak is obtained by extracting a single read or a small number of reads centered on the peak maximum from the processed two-dimensional electropherogram and using their sum.

4. Results and discussion

4.1. System performance

The important figures of merit of fluorescence detection systems include the LOD, separation efficiency and linearity. As fluorescein is a commonly used probe and allows comparisons to literature values, we use fluorescein to characterize the system. The least squares regression line for a log–log plot

of peak height versus fluorescein concentration from $5.0 \cdot 10^{-10}$ to $1.0 \cdot 10^{-7}$ M has a slope of 0.82 and a correlation coefficient (r^2) value of 0.98; the LOD is $4.8 \cdot 10^{-11}$ M or 29 000 molecules of fluorescein for a 1.0 nl injection. The separation efficiency of 230 000 is comparable to the value of 250 000 obtained previously using an on-line capillary detection system developed by our group [11], showing that the relatively slow readout rate of the CID and the post-column sheath flow system do not effect the efficiency greatly. While the CID readout rate of 1 Hz is slow compared to most single channel detection systems, the CID detector is an integrating detector. The slow readout rate can decrease the separation efficiency of narrow (<3 s) peaks. However, analyte peaks can not be missed by the detector because the CID is integrating all light falling on the array between the readouts.

This system is approximately two-orders of magnitude less sensitive than the most sensitive previously described wavelength-resolved fluorescence detection system developed in our group, in terms of both concentration and mass LODs [11]. The overall sensitivity of this system is, however, better than many commercial LIF detectors for CE. The major causes of the poorer sensitivity are the significantly higher read noise (even with the use of NDROs), and the lower collection efficiency caused by the higher spectral resolution and higher f-number of the Chromex spectrograph ($f/8$ instead of $f/2.2$). The optics and spectrograph of the present system have been chosen to provide the wavelength range from the ultraviolet (UV) to the near-infrared (IR) (200–800 nm), and the laser used has emission lines from 229–528 nm. A major advantage of the detector system is ability to cover the UV to IR regions by changing the spectrograph configuration through software commands instead of manually altering the setup.

4.2. Analysis of bilirubin in human serum

An example of using fluorescence emission spectral information involves the native fluorescence of a series of bilirubins. Bilirubin is a naturally fluorescent breakdown product of blood heme and is an important biological marker in the diagnosis, understanding and treatment of a variety of diseases associated with liver dysfunction [30]. Extremely high levels of bilirubin can lead to jaundice, where deposits of highly fat-soluble bilirubin form in the skin and eyes causing yellow discoloration [31]. The yellow color of bilirubin is indicative of its highly conjugated structure. This characteristic enables the detection of bilirubin using colorometric, fluorescence [32] and chemiluminescent methods [33]. Previously, we demonstrated the detection and separation of a series of bilirubins using the 457.9 nm line of an argon ion laser [32], although the 488 nm line can be used with a slight loss in sensitivity.

The analysis of bilirubin is complicated by the serum sample matrix. Although CE separation protocols have been developed that provide complete separation of the bilirubin isomers (unconjugated, monoconjugated, diconjugated and various biliproteins) from each other and matrix interferences using SDS, MeOH and BSA additives, [32] we did not completely optimize the separation in these experiments to demonstrate the ability to use fluorescence emission spectra to deconvolve several overlapped components. In this case, the different isomers of bilirubin are expected to have different spectral properties because of differing numbers of π-electrons.

The electropherogram obtained for an injection of human serum is shown in Fig. 5 and the fluorescence spectra of the labeled points are shown in Fig. 6. By visually comparing these spectra we observe that there are at least four species present, since only

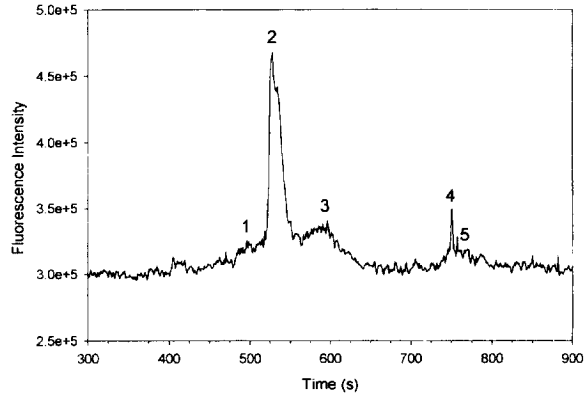

Fig. 5. Electropherogram of diluted human serum using 488 nm fluorescence excitation and summing the fluorescence emission from 505 to 614 nm.

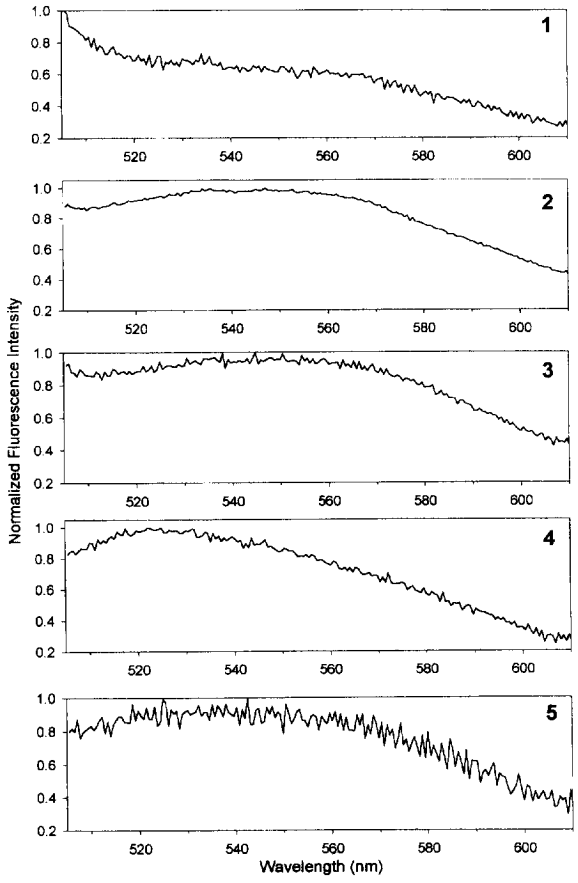

Fig. 6. Extracted fluorescence emission spectra from the electropherogram of human serum, with the numbers corresponding to the five labeled points in Fig. 5.

serum spectra 2 and 3 appear to be similar. To help identify the species in the serum sample, a bilirubin standard was separated under the same conditions and spectra of the resulting two peaks were extracted (Fig. 7). The observed spectra are consistent across each peak, so it is assumed that they represent two different bilirubin isomers. To make a better comparison of the standard and serum spectra, the variation in intensity due to concentration differences must be corrected. By dividing each spectrum by its maximum intensity, all of the spectra are normalized to the same scale. These spectra can then be compared by plotting them on the same axes, as is shown in Fig. 8 for standard peak 2 and serum peaks 1 and 3. Standard spectrum 2 and serum spectrum 3 closely match in the 560–600 nm region; to the blue of this wavelength, they are quite dissimilar, indicating serum peak 3 may be a different species or an incomplete separation and hence a combination of another species, such as serum peak 1.

The observed spectrum of a mixture is the linear combination of the individual spectra, so long as there is no spectral interference between them (i.e., one species does not absorb the fluorescence emission of another species that is present) [34]. For the example described above, this combination would take the form of:

$$\text{(Serum spectrum 2)} = X\text{(standard spectrum 2)} + Y\text{(serum spectrum 1)} + \epsilon \quad (1)$$

where X and Y are empirical scaling factors describing the combination of the normalized spectra and ϵ is an error factor. Based on this relationship, models to verify the presence of the bilirubin standards in the serum peaks are constructed. As one example:

$$\text{(Standard spectrum 2)}_{\text{FIT}} = \text{(serum spectrum 2)} - Z\text{(serum spectrum 1)} + \epsilon' \quad (2)$$

A routine using simplex optimization is written in MATLAB to determine the factors Z and ϵ' that minimize the error between the actual and modeled spectra of standard peak 2:

$$\epsilon_{\text{FIT}} = \sum[\text{(standard spectrum 2)} - \text{(standard spectrum 2)}_{\text{FIT}}]^2 \quad (3)$$

The validity of the fit is checked by calculating the correlation coefficient, r^2:

$$r^2 = \frac{\sum_{i=1}^{n}(R_i' - \bar{R})^2}{\sum_{i=1}^{n}(R_i - \bar{R})^2} \quad (4)$$

where R_i' is the modeled spectrum, R_i is the standard spectrum and $\bar{R}$ is the mean value of the standard spectrum, R_i [34]. Fig. 9 shows the results for the fit described above along with those for combinations of serum peaks 2 and 3 with standard peak 2. By examination of the plots along with the r^2 values it can be seen that serum peaks 2 and 3 may be

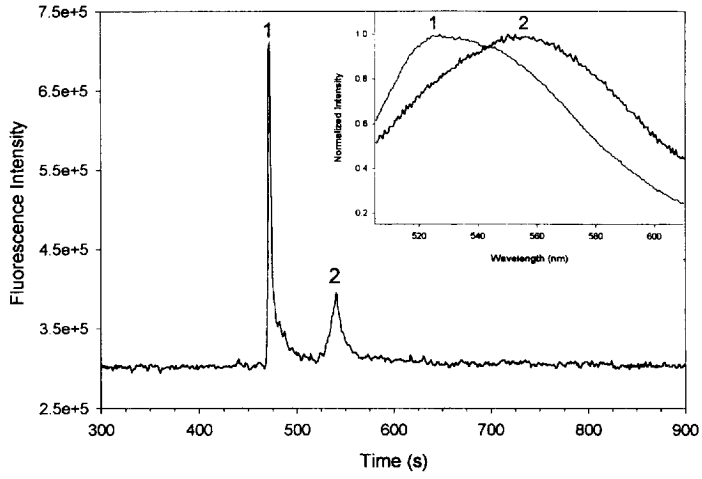

Fig. 7. Electropherogram of bilirubin standard using 488 nm fluorescence excitation and summing the fluorescence emission from 505 to 614 nm. The inset shows the spectra from the two labeled points.

combinations ($r^2 = 0.90$ and 0.92, respectively) of the bilirubin standard with serum peak 1.

The elution time of serum peak 4 does not correspond to those of either of the peaks seen in the bilirubin standard separation (see Figs. 5 and 7). When the spectrum of serum peak 4 is examined, however, similarities to the spectrum of standard peak 1 can be seen (see Figs. 6 and 7). Performing a spectral fit of serum peaks 4 and 5 with standard peak 1 results in an r^2 value of 0.84. While it is difficult to say that this peak is a combination of the two modeled components, it could be an isomer of bilirubin that was not present in the standard. The discrepancy in the fit may also be increased due to the low signal intensity of the spectrum of serum peak 5, resulting in magnification of the background noise during the spectral normalization.

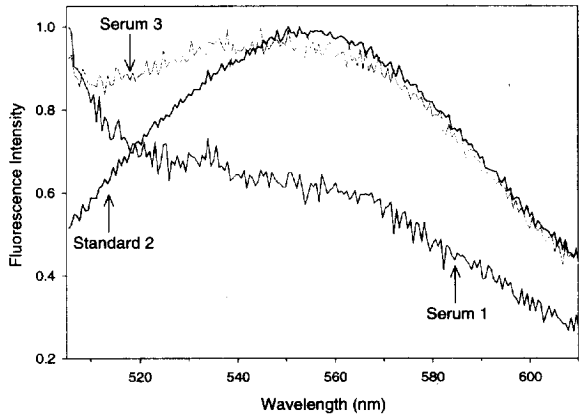

Fig. 8. Superimposed and normalized spectra from Figs. 6 and 7 (serum 1 and 3 and standard 2).

We have shown that fluorescence emission spectra can be used to indicate whether electrophoretic peaks are due to multiple components, and have attempted to match analyte peaks based on spectral properties. Many of the data manipulation techniques developed for DAD detection in CE can likely be transferred to wavelength resolved fluorescence detection in order to provide additional information on peak purity, electrolyte composition and multi-component analysis. Fluorescence is an environmentally sensitive technique, so that fluorescence emission spectra can also provide information on separation pH [35], ionic strength and composition. As the availability of detector arrays such as charge injection device and charge-coupled device arrays becomes more widespread, we expect the use of wavelength resolved fluorescence detection to increase.

Acknowledgements

The support of the National Science Foundation (CHE 96-22663) and NIH (NS31609) are gratefully

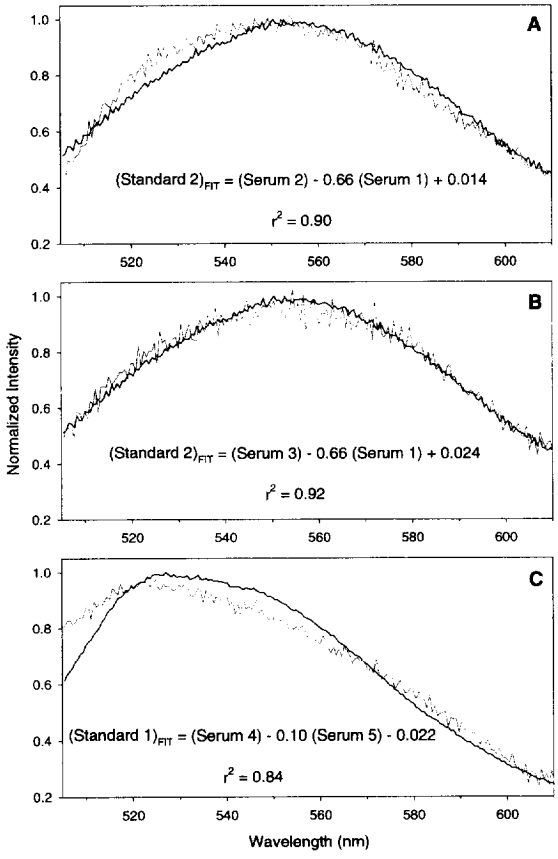

Fig. 9. (A) Fit of serum 2–serum 1 (grey) superimposed on bilirubin standard 2 (black). (B) Fit of serum 3–serum 1 (grey) superimposed on bilirubin standard 2 (black). (C) Fit of serum 4–serum 5 (grey) superimposed on bilirubin standard 1 (black).

acknowledged, as is a Sloan Fellowship support to J.V.S. and a Colgate-Palmolive award to X.X.

References

[1] J.W. Jorgenson, K.D. Lukacs, Science 222 (1983) 266.
[2] J.P. Landers, Handbook of Capillary Electrophoresis, CRC Press, Boca Raton, FL, 2nd ed., 1997, pp. 384, 485.
[3] R. Weinberger, Practical Capilllary Electrophoresis, Academic Press, New York, 1993, pp. 67, 229.
[4] R.L. St. Claire, III, Anal. Chem. 68 (1996) 569R.
[5] J.A. Jankowski, S. Tracht, J.V. Sweedler, Trends Anal. Chem. 14 (1995) 170.
[6] H.K. Kristensen, Y.Y. Lau, A.G. Ewing, Neurosci. Methods 51 (1994) 183.
[7] R.T. Kennedy, M.D. Oates, B.R. Cooper, B. Nickerson, J.W. Jorgenson, Science 246 (1989) 57.
[8] B.L. Hogan, E.S. Yeung, Anal. Chem. 64 (1992) 2841.
[9] E. Gassman, J.E. Kuo, R.N. Zare, Science 230 (1985) 813.
[10] D.Y. Chen, K. Adelhelm, X.L. Cheng, N.J. Dovichi, Analyst 119 (1994) 349.
[11] A.T. Timperman, K. Khatib, J.V. Sweedler, Anal. Chem. 67 (1995) 139.
[12] R.A. Keller, W.P. Ambrose, P.M. Goodwin, J.H. Jett, J.C. Martin, M. Wu, Appl Spectrosc. 50 (1996) 12A.
[13] N.J. Dovichi, J.C. Martin, J.H. Jett, M. Trkula, R.A. Keller, Anal. Chem. 56 (1984) 348.
[14] F. Zarrin, N.J. Dovichi, Anal. Chem. 57 (1985) 2690.
[15] J.Z. Zhang, D.Y. Chen, S. Wu, H.R. Harke, N.J. Dovichi, Clin. Chem. 37 (1991) 1492.
[16] M.J. Sepaniak, D.F. Swaile, A.C. Powell, J. Chromatogr. 480 (1989) 185.
[17] S. Kobayashi, T. Ueda, M. Kikumoto, J. Chromatogr. 480 (1989) 179.
[18] S.K. Yeo, H.K. Lee, S.E.Y. Li, J. Chromatogr. 585 (1991) 133.
[19] D.F. Swaile, M.J. Sepaniak, J. Microcol Sep. 1 (1989) 155.
[20] Y.F. Cheng, R.D. Piccard, T. Vo-Dinh, Appl. Spectrosc. 44 (1990) 755.
[21] S. Xiong, J. Li, C. Jieke, Anal. Chim. Acta 322 (1996) 187.
[22] A.T. Timperman, K.E. Oldenburg, J.V. Sweedler, Anal. Chem. 67 (1995) 3421.
[23] A.T. Timperman, J.V. Sweedler, Analyst 121 (1996) 45R.
[24] Y.F. Cheng, S. Wu, D.Y. Chen, N.J. Dovichi, Anal. Chem. 62 (1990) 496.
[25] Q. Li, E.S. Yeung, Appl. Spectrosc. 49 (1995) 825.
[26] J.V. Sweedler, R.B. Bilhorn, P.M. Epperson, G.R. Sims, M.B. Denton, Anal. Chem. 60 (1988) 282A.
[27] J.V. Sweedler, K.L. Ratzlaff and M.B. Denton, Charge Transfer Devices in Spectroscopy, VCH Publishers, New York, 1994, p. 50.
[28] J.V. Sweedler, CRC Crit. Rev. Anal. Chem. 24 (1993) 59.
[29] K.R. Ratzlaff, Introduction to Computer Assisted Experimentation, Wiley, New York, 1987, p. 384.
[30] J.R. Chowdhury, A.W. Wolkoff and I.M. Arias, in C.R. Scriver, A.L. Beaudet, W.S. Sly and D. Valle (Editors), The Metabolic Basis of Inherited Disease, McGraw-Hill, New York, 6th ed., 1989, p. 1367.
[31] D. Voet and J.G. Voet, Biochemistry, Wiley, New York, 1990, p. 706.
[32] N. Wu, J.V. Sweedler, M. Lin, J. Chromatog. B 654 (1994) 185.
[33] L.P. Palilis, A.C. Calokerinos, N. Grekas, Anal. Chim. Acta 333 (1996) 267.
[34] M.A. Sharaf, D.L. Illman and B.R. Kowalski, Chemometrics, Wiley, New York, 1986, p. 166.
[35] A.T. Timperman, S.E. Tracht, J.V. Sweedler, Anal. Chem. 68 (1996) 2693.